Finite element analysis of levee stability for flood early warning systems

Melnikova, N.B.

Publication date
2014

Chapter 5 Boston dike case study: simulation and validation of a coupled flow-structure interaction model under tidal loads[4]

The first scientific question raised in this research was check of a principal ability of an earthen dike computational model to adequately simulate complex physical processes occurring at failure and correctly predict failure under prescribed loads. The Boston levee validation test site has become the next step towards the positive answer to this question and a platform for cross-validation of three computational models for dike stability assessment: the *Virtual Dike* model, a finite element model built in the commercial software package Plaxis and a limit equilibrium analysis model based on the Bishop's method.

5.1 Test site description and ground conditions

The earthen levee at Boston, a town on the east coast of England at high risk of flooding, is known for a history of frequent toe slippages on the river side. This mechanism is presumably caused by high pore water pressures remaining in the dike when the river water recedes. The dike forms the right bank of the River Haven, which has a tidal range of about 6 m. The crest level of the dike is at 6m above the mean sea level; the deepest part of the river bed is at 2m from the mean sea level. The site is predominately grassed with several trees (Figure 5-1a). It has suffered from instability at the toe along the majority of its length (Figure 5-1b).

(a) (b)

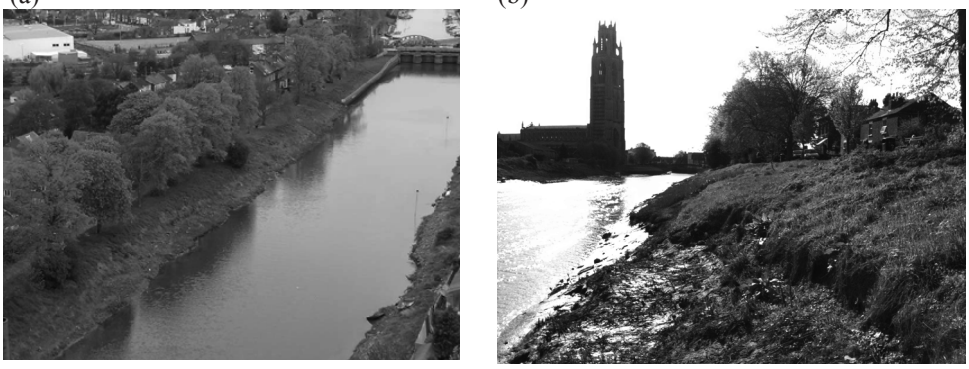

Figure 5-1 (a) Boston levee location at the right bank of the river Haven; (b) View of embankment with signs of toe slippage

[4] Parts of this chapter have been published in (Melnikova, N.B., Jordan, D., Krzhizhanovskaya, V.V., Sloot, P.M.A. (2014). Slope instability of the earthen dike in Boston, UK: numerical simulation and sensor data analysis. Submitted to Journal of Computational Science, Elsevier)

The area was investigated in 2010 as part of the Boston Barrier Phase 1 Ground Investigation, this included a single borehole within the study dike. Further boreholes and Cone Penetration Tests were carried out as part of the installation of the sensors for the UrbanFlood Project. From the investigation, the variation in ground conditions across the site may be summarized as shown in Figure 5-2; beneath made ground and a thin layer of fine sand, lies some 5m of soft to firm alluvial clays. These in turn overlie sands and stiff boulder clay. The obtained soil parameters are presented in Table 5-1. Sensor locations are specified in Figure 5-2 relative to the Ordnance Datum (OD), which is the reference sea level in Great Britain (defined as the mean sea level at Newlyn in Cornwall between 1915 and 1921).

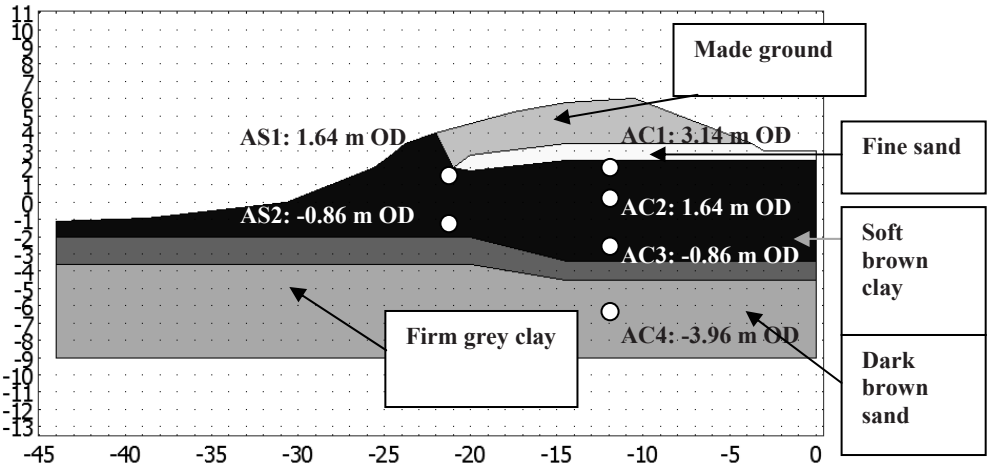

Figure 5-2. Scheme of the cross-section A: soil build-up and sensors elevations, metres from Ordnance Datum

Table 5-1. Summary of soil parameters for the Boston levee

Property	Made ground	Fine sand	Soft brown clay	Dark brown sand	Firm grey clay
Hydraulic conductivity, m/day	10	1	0.01	10	0.01
Van Genuchten parameter α, 1/m	2	2	0.5	-*	-
Van Genuchten parameter n	1.5	1.5	1.5		
Saturated water fraction	0.4	0.4	0.43		
Residual water fraction	0.045	0.045	0.3		
Density dry kN/m3	19.5	17.5	-		
Density wet kN/m3	-		18	22	18

Effective Young's modulus, MPa	18	28	2	18	2
Effective Poisson's ratio	0.35	0.3	0.35	0.3	0.3
Effective cohesion, kPa	5	0	2	0	5
Friction angle, grad	30	28	25	27.6	23.5

*Table cells containing "-" refer to the properties not used in corresponding soil strata. For example, Van Genuchten parameters for dark brown sand and firm grey clay were not used in simulation because these soil strata stay saturated during tide oscillations.

5.2 Instrumentation and sensor data analysis

The dike has been equipped at each of two cross-sections with six GeoBeads MEMS (micro-electro-mechanical) sensors registering pore pressure and media temperature. Differences in temperature measurement curves strongly indicate water flow through the soil - any drop in sensor temperature might be an indication of the development of piping. The Geobeads sensors have been installed in boreholes in the two planar transversal cross-sections (depicted as A and B in Figure 5-3). Positions of the GeoBeads sensors in the cross-section A are shown in Figure 5-2; vertical elevations are specified relative to the Ordnance Datum. Sensors AC1-AC4 are of increasing depth at the crest of the bund whilst sensors AS1-AS2 are located at about mid-slope height.

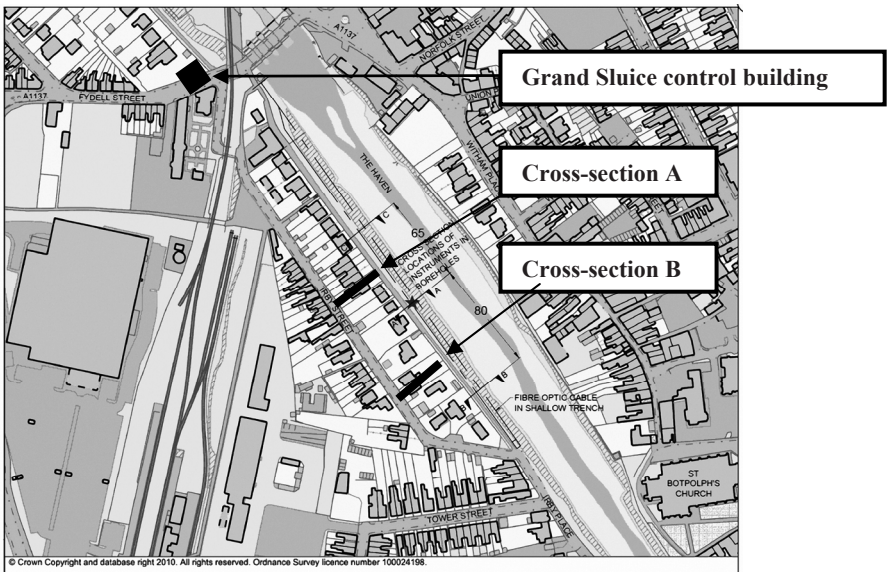

Figure 5-3. Boston levee site, with the cross-section locations

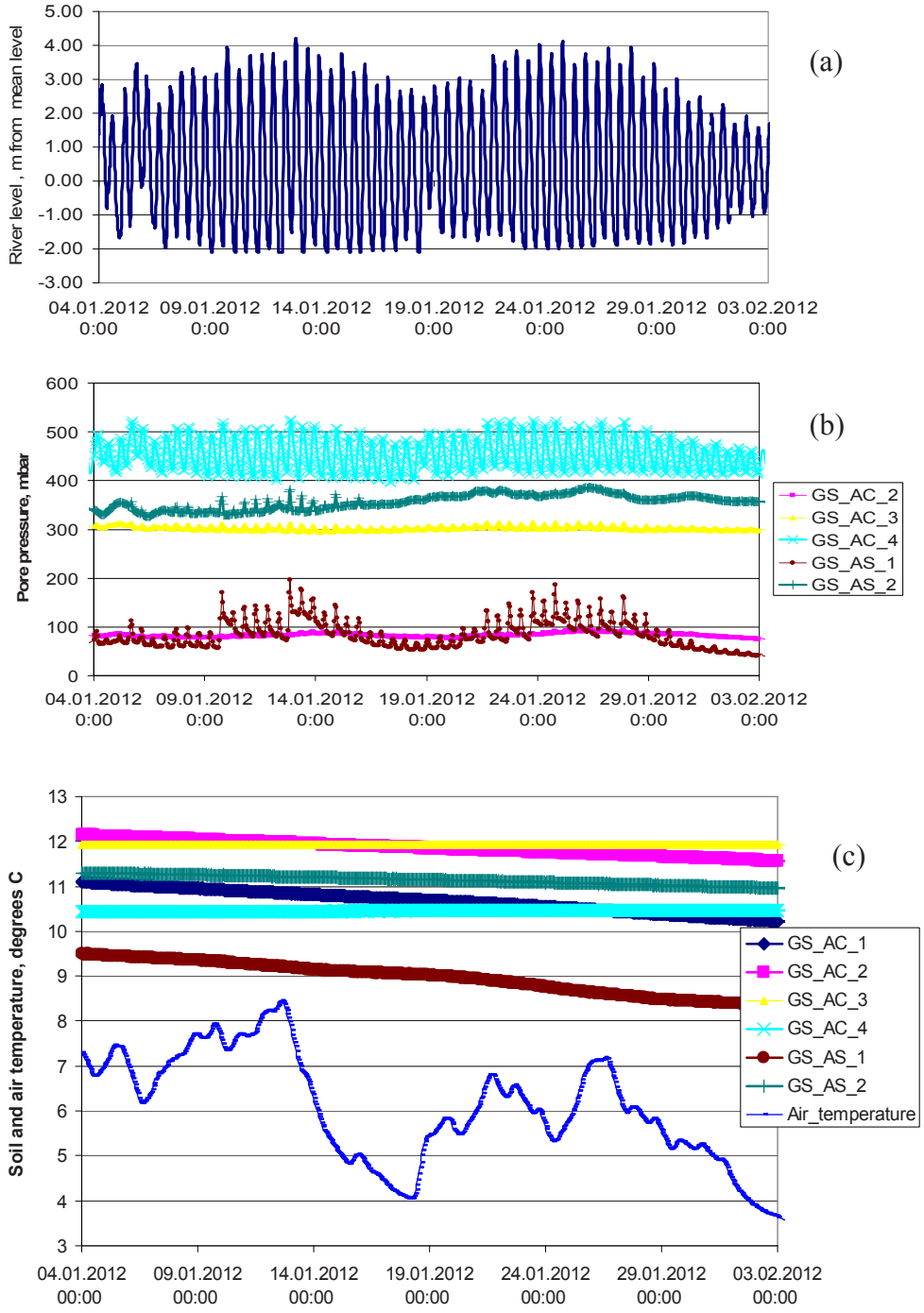

Figure 5-4. (a) river level dynamics; (b, c) sensor readings: (b) pore pressure; (c) medium temperature

The instrumentation and control building for the Grand Sluice on Haven River provided an ideal location for situating the computer equipment and providing power to the sensors. The use of mains power eliminated the need to replace batteries and reduced the level of maintenance required on the sensor equipment, ensuring uninterrupted data signals. The control building is located at 129 m distance upstream from cross-section A and is shown in the top of Figure 5-3 near the bridge with the sluice.

Sensor readings in the Boston levee had been previously analyzed in (Simm et al., 2012a), for a period of one year since the installation of sensors in May 2011. In the present research we focus on the response of the dike to tidal loading (putting aside slow seasonal processes), so we analyzed sensor data and dike stability for a one-month period in January 2012. The readings in cross-section A are presented in Figure 5-4; these are: water level dynamics in the river Figure 5-4a; pore pressure readings (Figure 5-4b) and water and air temperature readings (Figure 5-4c).

The results show a good response to tidal variations particularly in AS1, the upper sensor on the slope. Plateau-like segments of the AS1 curve correspond to the low-tide phases: the large soft brown clay layer stays saturated even at a low-tide phase (when the river bed is almost dry) - hence the pressure distribution and hydraulic load in the clay layer do not change during the low-tide phase. There is no significant time-lag between the tide and piezometric levels. The tidal range in mid-river is about 6m whilst the AS1 pressure head range is about 1m (100 mbar). This limited magnitude of response reflects the position of the piezometers within the slope relative to the maximum tidal variation in the centre of the river channel. It is considered that the piezometers are measuring an undrained elastic response in the soil-water continuum due to the loading caused by variation in water levels in the adjacent river channel. The assumption on the undrained state of the clay stratum is confirmed by comparing mean pressure heads measured by sensors in the soft brown clay stratum with pressure heads in the river and in the underlying dark brown sand layer (the comparison is discussed below).

According to sensor readings, AC1 is located in a dry zone above the ground water level, which is why it is not shown in Figure 5-4b. AC2 and AC3 sensors located in the soft clay layer far from the river-side slope are almost insensitive to the tide. Mean value of pore pressure oscillations (relative to atmospheric pressure) in sensors AC2 and AS1 is about 90 mbar. Both sensors are located at the same elevation of 1.64 metres above OD – so the mean ground water table in the dike is at 2.54 m above OD. According to the soil build-up scheme (Figure 5-2), the phreatic line goes through the thin layer of fine sand.

AC4 naturally produces high response to the tidal loading due to high conductivity of the dark brown sand layer where the sensor is placed. Mean pore pressure in AC4 is 450 mbar and its elevation is 3.96 m below OD, which gives mean value of total head +0.54 m above OD. This value agrees with the mean river level (Figure 5-4a), which is 0.6 for the considered period of time, proving that the dark brown sand layer is hydraulically connected to the river. As it was mentioned above, in the upper layers of soft brown clay, fine sand and made ground, the mean total head is at 2.54 m above OD which is two meter higher than in the underlying sand layer. This discrepancy confirms the assumption that the clay layer and the overlying soil layers (fine sand, made ground) are hydraulically isolated both from the foundation sand layer and from the river due to low permeability of clay. The

massive clay layer retains large amount of water coming with precipitation which is most intensive during winter time.

Soil and air temperature curves measured by sensors are shown in Figure 5-4c. At winter, the soil temperature is naturally higher than the air temperature, due to the high heat capacity of soils. Sensor AS1 produces minimal temperature values as it is closer to the land surface than the other sensors. AC1-AC2 and AS1-AS2 temperatures gradually decrease during the month, together with the dynamics of the mean air temperature value (and presumably of the water temperature in the river). Sensors AC3-AC5 located in deep soil strata below the ground water level produce nearly constant values of temperature around 10-12°C.

In the case of piping erosion in the dike, temperature sensors can provide warning information: decrease of local temperature value from expected soil temperature to the water temperature indicates that piping is occurring in the dike (Pyayt et al., 2014). However piping has never been visually observed or sensor detected at this site. As it was mentioned above, the dike is prone to occasional river-side toe slippages, such as shown in Figure 5-1b. There is no data available from the maintenance records about the precise moments in time when these local slippages occurred.

A detailed analysis of Boston site sensor data has been reported in (Pyayt et al., 2013a), where a data-driven approach with a neural network were applied for modelling a transfer function between the sensors within the Artificial Intelligence software module.

5.3 Mathematical models and numerical implementation

For the analysis of the Boston levee stability, two approaches have been employed: finite element modelling and limit equilibrium method. Below we separately describe mathematical models and numerical solution procedures for the two approaches.

5.3.1 Finite element model

In FEM analysis, a one-way coupled fluid-to-structure interaction model for the planar cross-section of the dike has been considered.

Water flow through the porous media is described by Richards' equation (2.12) with the Van Genuchten model (2.4)-(2.6) for water retention in vadose zones. Specific moisture capacity C and relative permeability k_r in the unsaturated zone are defined as functions of the effective water content (Van Genuchten, 1980).

The mechanical sub-model describes stress-strain state of the dike under hydraulic load, gravity and volumetric pore pressure load obtained from flow simulation. Linear elastic perfectly plastic strains of the soil skeleton are described by the general equations of plastic flow theory: (2.13) for drained behaviour, (2.19) - for undrained behaviour.

In the present work, we omitted pore suctions when calculating effective stresses above the phreatic line, assuming effective stresses to be equal to total stresses in the vadose zone. This assumption was based on the piezometers readings (see section 5.2 for details), which showed that the clayey part of the Boston levee volume stays fully saturated

during tidal cycles, while a vadose zone exists on top of the dike in the loose, coarse-grained stratum built from the mixture of soil and debris and thus producing quite low suctions ("made ground" stratum in Figure 5-2):

$\underline{\underline{\sigma}} = \underline{\underline{\sigma}}_{eff} - p\underline{\underline{I}}$ in saturated zones, $\underline{\underline{\sigma}} = \underline{\underline{\sigma}}_{eff}$ in vadose zones.

Plastic flow has been modelled with a modification of the Drucker-Prager plasticity model, optimized for plane strain problems by providing the best smooth approximation of the Mohr-Coulomb surface in the stress space (Chen and Mizuno, 1990):

Equations (2.12)+(2.13) form a one-way coupled flow-structure interaction systems, where the porous flow sub-model generates a volume load (computed as pore pressure gradient) for the mechanical sub-model.

Boundary conditions for fluid and mechanical sub-models are schematically shown in Figure 5-5a,b.

Hydraulic boundary conditions are listed below:

- Black line (Figure 5-5a) - the river side, pressure boundary condition: $\begin{cases} p = \rho g \cdot (h(t) - y) \quad for \quad y \le h(t), \\ p = 0 \quad for \quad y > h(t) \end{cases}$, where *h(t)* is river level, metres;
- Cyan line (Figure 5-5a) - the land side, pressure boundary condition: $\begin{cases} p = \rho g \cdot (h_L(t) - y) \quad for \quad y \le h_L(t), \\ p = 0 \quad for \quad y > h_L(t) \end{cases}$, where $h_L(t)$ is ground water level at the land side;
- Magenta line shows impervious walls.

Ground water table at the land side was specified using mean values of AC2 and AC4 pore pressure readings discussed in the previous section. For the dark brown sand and firm grey clay layers, h_L= 0.5 m; for the soft brown clay layer and overlying layers, h_L= 2.5 m.

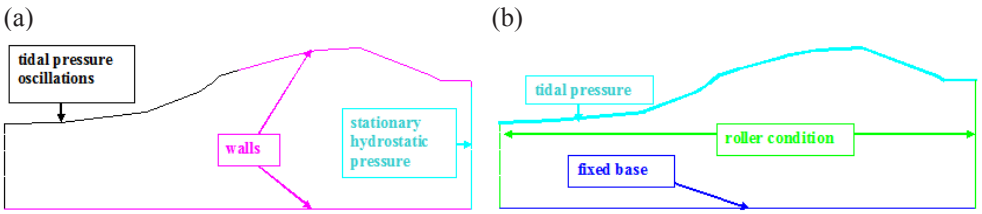

Figure 5-5. Boundary conditions; (a) fluid sub-model; (b) mechanical sub-model

Mechanical boundary conditions have been specified as follows:

- Cyan line (Figure 5-5b) - free surface with total normal stress specified: $\underline{n} \cdot \underline{\underline{\sigma}} = -\rho g \cdot (h(t) - y)$ *for* $y \le h(t)$; $\underline{n} \cdot \underline{\underline{\sigma}} = 0$ *for* $y > h(t)$;
- Green line - roller condition: normal displacements and shear stresses are zero U_x=0, $\sigma_{xy} = 0$;
- Blue line - fixed condition: zero displacements $\underline{U} = 0$.

The overall solution procedure includes two loading stages:

1) Gravity settlement problem solution with stationary hydraulic boundary conditions (see section 5.4 for details). Gravity load and buoyancy load were applied incrementally to an initially stress-free domain. Mechanical behaviour of clay layers (brown soft clay and firm grey clay) was simulated as "drained" at this stage. Stresses obtained at this stage were used in the next stage to define pre-stresses in the domain.

2) Tidal mode simulation. Initial condition: pore pressures and stresses are obtained from the previous completed stage; displacements are zero. At each physical time step, a filtration problem was solved with a time-dependent FE solver; than the obtained pore pressures were passed to the mechanical sub-model as volume load. Increments of hydraulic loads were computed and gradually applied in the incremental parametric solver. Mechanical behaviour of clay layers was simulated as undrained at this stage; the undrained analysis was performed on the basis of the effective strength parameters (the procedure was described in section 2.4.2).

For each tide phase, strength reduction factors *SRF* were calculated according to the procedure described in paragraph 2.3.

A two-dimensional finite element mesh was composed of 6328 second-order triangular elements (Figure 5-6), this mesh was used for both fluid and mechanical analysis. High density of mesh is caused by using highly nonlinear Van Genuchten rheological model for variably saturated soil.

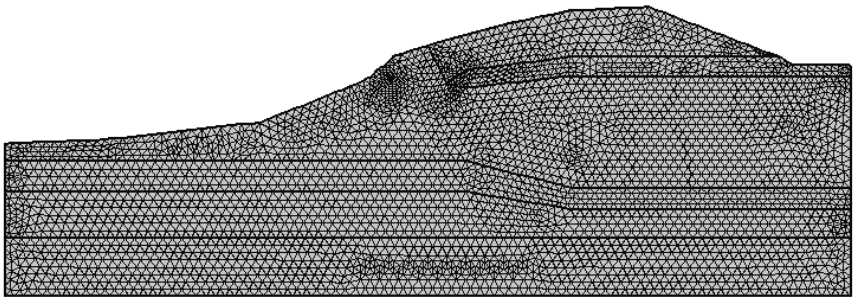

Figure 5-6. Boston levee model - finite element mesh

The functionality of the Comsol package supports multi-physics coupling – the equations describing the time-dependent fluid sub-model and the quasi-static mechanical

sub-model can be united in one system, which will be integrated by a time-dependent solver. However, convergence of the time-dependent solver was poor for the highly-nonlinear mechanical sub-model: integration in time-domain required very small time-steps and finally stopped at divergence of non-linear iterations. Typically plastic deformation problems in Comsol require a parametric solver for their solution. That's why a two-step solution scheme described in Figure 3-2 was used.

5.3.2 Limit equilibrium model

The *Geo-Stability* software package has been used for the limit equilibrium analysis. This uses the well known Bishop method of slices (Bishop, 1955b) to calculate the factor of safety of the dike's slope.

By assuming varying groundwater profiles within the dike for varying external water conditions, the module was able to provide a matrix of factors of safety for varying water levels (see Table 5-2 in the next section). This matrix of results relates external water levels and pore pressures (as measured in the sensors) with factor of safety. Additional values of factor of safety are then determined by an interpolation routine that finds intermediate values between those within the look-up table. Development of such stability matrices or look-up tables that could be interrogated using actual sensor values significantly simplified the process of using sensor information compared to the approach originally envisaged. Hence, the look-up table approach has been adopted within the study.

5.4 Finite element simulation results

First, fluid sub-model of the Virtual Dike FEM model has been calibrated using pore pressure sensors recordings. The river level dynamics within the training period considered for calibration is presented in Figure 5-7a. Hydraulic conductivity of the dark brown sand layer has been adjusted so that the amplitude and time lag of simulated pressure oscillations agree with those registered by the AC4 sensor (Figure 5-7b). The calibrated value of conductivity is given in Table 5-1. Calibration of the soft brown clay conductivity was not performed due to undrained condition of the layer. The calibrated Virtual Dike FEM model then was used for stability analysis.

The first stage of the stability analysis was gravity settlement simulation. Clay behaviour was simulated as drained at this stage. The boundary conditions were stationary: in dark brown sand and firm grey clay layers, both river level and land side ground water level were equal to h_L= 0.5 m (value based on the AC4 pressure sensor readings); in soft brown clay layer and the overlying layers h_L= 2.5 m (based on the AC2 and AC3 pressure measurements). Initial condition was specified as follows: vadose zones (made ground, fine sand): p=-5 kPa; saturated zones (soft brown clay with the underlying layers): hydrostatic pore pressure distribution according to water tables specified in the boundary conditions. During simulation period of 10 days pore pressures reached steady-state condition (Figure 5-8a). Gravity settlement of the dike under these hydraulic loads was 0.355 m (Figure 5-8b).

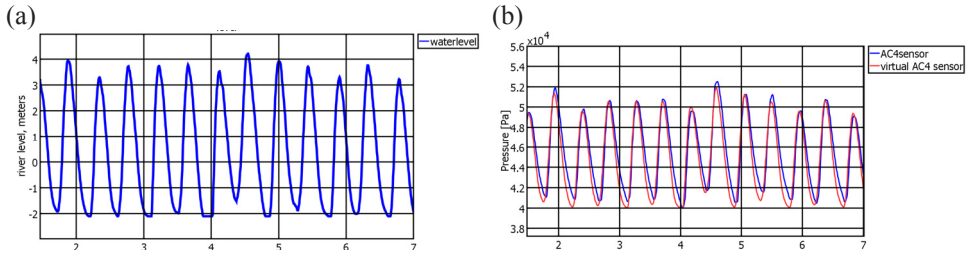

Figure 5-7. Dark brown sand layer conductivity calibration: (a) river level dynamics during training period; (b) comparison of real and simulated signals in AC4 sensor

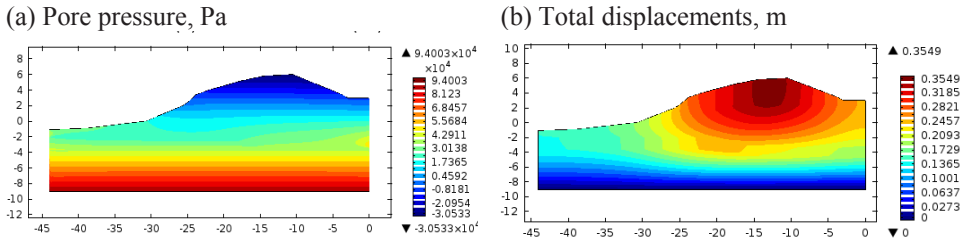

Figure 5-8. Gravity settlement simulation results; (a) pore pressure; (b) total displacements

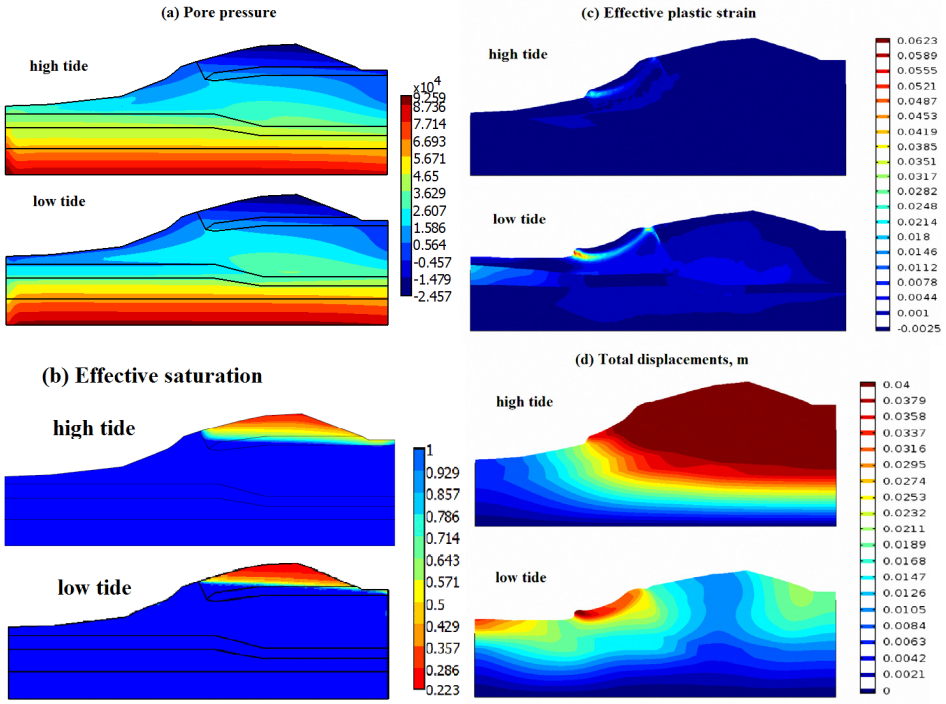

Figure 5-9. Tidal mode simulation (a) pore pressure; (b) effective saturation; (c) effective plastic strains (displ. scaling factor 50); (d) total displacements: (displ. scaling factor 50)

Resulting distributions of pore pressure and stresses were then used as starting point for the subsequent pre-stressed tidal mode analysis. In the tidal mode, clay behaviour was simulated as undrained. River-side boundary conditions in the fluid and mechanical sub-models were non-stationary (see section 5.3.1 for their specification).

Figure 5-9a gives the pore pressure distributions at high tide and low tide phases. In the clay layer, it is only a local zone at the river slope that reacts to tidal oscillations. Maximal response to the tide is naturally observed in the dark brown sand layer. Effective saturation distribution changes very little with the tide and looks similar for the low tide and high tide phases (Figure 5-9c) - the thick layer of soft clay located between the levels of -2 m and +4 m does not really change saturation during relatively fast diurnal oscillations, hence the hydraulic load in clay does not change much from high tide to low tide.

Effective plastic strain distributions in the deformed domain are presented in Figure 5-9b for high tide and low tide phases. Effective plastic strain characterizes intensity of plastic strains and is calculated from the components of plastic strain rate tensor by formula:

$$\varepsilon_p = \int_0^t \dot{\varepsilon}_p dt, \quad \dot{\varepsilon}_p = \frac{\sqrt{2}}{3}\sqrt{(\dot{\varepsilon}_{px} - \dot{\varepsilon}_{py})^2 + (\dot{\varepsilon}_{px} - \dot{\varepsilon}_{pz})^2 + (\dot{\varepsilon}_{pz} - \dot{\varepsilon}_{py})^2 + 6\dot{\varepsilon}_{pxy}{}^2 + 6\dot{\varepsilon}_{pxz}{}^2 + 6\dot{\varepsilon}_{pyz}{}^2}$$

Simulations have converged, indicating that the dike is stable under the tidal load. However, formation of a shallow slip surface located entirely in the soft clay layer can be seen at the low tide (Figure 5-9c).

Total displacements distributions are shown in Figure 5-9d. At high tide, total displacements are mostly produced by vertical flotation of the dike; at low tide, the slip surface formation is clearly identified at the river slope.

5.5 Limit equilibrium modelling results

Safety factors obtained in the *Geo-Stability* LEM analysis are presented in Table 5-2, in the form of a look-up table with variable river levels (RL) and ground water levels (GWL) within the dike. Columns AC1-AS2 show pore pressure values calculated at sensor locations. In the limit equilibrium analysis, the phreatic line shape was determined as a straight line connecting river and land side water levels. This simplification caused a significant difference in the distribution of pore pressures and soil weights in the dike, compared with the FEM modelling results, as the clay layer is less saturated in LEM for the most of the GWL conditions.

Figure 5-9c from the previous paragraph shows that the FEM is predicting at low tide an approximately circular failure surface, thus proving that use of the LEM is appropriate, though because of the simplifications required modelling for the latter different results were obtained from the two methods – see section 0.

The lowest value of the Factor of Safety FoS =1.04 has been obtained for the combination of the low tide condition RL = 0m with the highest ground water levels (GWL = 4m and GWL = 6m). This fact confirms the conclusion made from the FEM simulation

results presented in the previous section: the less stable mode corresponds to the combination of maximal saturation of the dike with the low-tide water levels.

Slip surfaces (circles) obtained by Bishop's method for the high tide phase (RL=4 m, GWL=0 m) and for the low tide phase (RL=-1.1 m, GWL=0 m) are shown in Figure 5-10b,d. The slip surfaces are shallow, with the high-tide slip circle having much larger radius than the low-tide circle. The shape of the low-tide slip surface agrees well with the real-life slippage observations.

Table 5-2. Stability factor values for various hydraulic conditions

		Simulated relative pore pressure, in sensor locations, cross-section A (Atmos=0kPa)							
River level (RL)	**Assumed ground water level (GWL)**	**AC1**	**AC2**	**AC3**	**AC4**	**AC5**	**AS1**	**AS2**	**Safety factor**
[m]	**[m]**	**[kPa]**							**[-]**
-1.1	0	Atmos	Atmos	8	39	63	Atmos	7.94	1.55
0	0	Atmos	Atmos	8	39	63	Atmos	7.94	1.52
0	2	Atmos	3	28	59	83	2.94	27.94	1.28
0	4	8	23	48	79	103	22	47	1.04
0	6	28	43	68	99	123	22	47	1.04
2	0	Atmos	Atmos	8	39	63	Atmos	7.94	1.67
2	2	Atmos	3	28	59	83	2.94	27.94	1.55
2	4	8	23	48	79	103	22	47	1.08
2	6	28	43	68	99	123	22	47	1.08
4	0	Atmos	Atmos	8	39	63	Atmos	7.94	2.11
4	2	Atmos	3	28	59	83	2.94	27.94	2.11
4	4	8	23	48	79	103	22.94	47.94	1.88
4	6	28	43	68	99	123	22.94	47.94	1.60

5.6 Models cross-validation: comparison of FEM and LEM results

Within the *UrbanFlood* project, three independent models of the Boston levee were designed (Krzhizhanovskaya et al., 2012). These were: our *Virtual Dike* finite-element model, the limit equilibrium model from HR Wallingford and a finite-element model developed in Plaxis software by Siemens. Comparison of the results obtained by different tools for the low-tide and high-tide phases is presented in Table 5-3. Ground water level (GWL) was set at 2.5 m (based on sensor measurements). River level (RL) during high tide was +4 m above mean sea level; at low tide, RL was -1.1 m. For the cross-validation of LEM and FEM models, factors of safety for GWL=2.5 m have been obtained by interpolating between values in Table 5-2.

The values of strength reduction factors *SRF* obtained in Virtual Dike and in Plaxis by strength reduction method agree very well (the difference is 6% and 5% for high tide and low tide, respectively). The values of *FoS* obtained in Geo-Stability LEM program are much higher (by 22% at low tide and by 100% at high tide).

Table 5-3. Safety factors calculated by *Virtual Dike*, Plaxis and *Geo-Stability*

High tide (RL=4 m, GWL=2.5 m)			**Low tide (RL=-1.1 m, GWL=2.5 m)**		
Virtual Dike **(FEM)** ***SRF***	***Plaxis*** **(FEM)** ***SRF***	***Geo-Stability*** **(LEM)** ***FoS***	***Virtual Dike*** **(FEM)** ***SRF***	***Plaxis*** **(FEM)** ***SRF***	***Geo-Stability*** **(LEM)** ***FoS***
1.04	1.10	2.05	1.03	1.08	1.26

Values of SRF obtained by FEM do not significantly differ for the high tide (RL=4 m) and for the low tide (RL=-1.1 m). This is due to the fact that a thick layer of soft clay located between the levels of -2 m and +4 m OD at the river slope has low permeability and does not significantly change saturation during relatively fast diurnal oscillations (see Figure 5-9b). We believe that in reality the hydraulic load changes quite insignificantly with the tide due to the large amount of clay in the dike (this is confirmed by sensor readings in Figure 5-4b) and this effect has been reproduced in the more realistic FEM simulation. In the case of continuous rainfall infiltration, the stability factors will most likely decrease due to saturation of the top made ground layer and the increase in the weight of the dike, which can result in slope slippage.

In *Geo-Stability* LEM analysis, hydraulic loads differ significantly for the high tide and low tide, as the ground water table was assumed to be a straight line connecting river and landside water levels. Due to the same reason, the difference between high and low tide critical slip surfaces in Geo-Stability (Figure 5-10b,d) is much higher than in the Virtual Dike (Figure 5-10a,c).

In all models, the critical slip surface is shallow. For the high tide, it ends slightly above the river side toe of the dike, while for the low tide, the radius of the surface increases and slip surface ends below the river side toe. The radiuses of slip surfaces increase from high tide to low tide, both in Virtual Dike and in Geo-Stability programs. However, in the Virtual Dike FEM model the critical surfaces are located entirely within the soft clay layer whilst in the Geo-Stability LEM model they cross the fine sand and made-ground layers.

Distributions of total displacements obtained in Plaxis and in Virtual Dike qualitatively agree (see Figure 5-11). However the values of maximal displacements differ. The difference is due to the added value of the dynamical (time-dependent) simulations in the porous flow sub-model, compared to the static calculation in Plaxis. The other possible reason of this difference is use of different constitutive models of plasticity: classic Mohr-Coulomb plasticity model used in Plaxis via 2D Drucker-Prager approximation model in Virtual Dike.

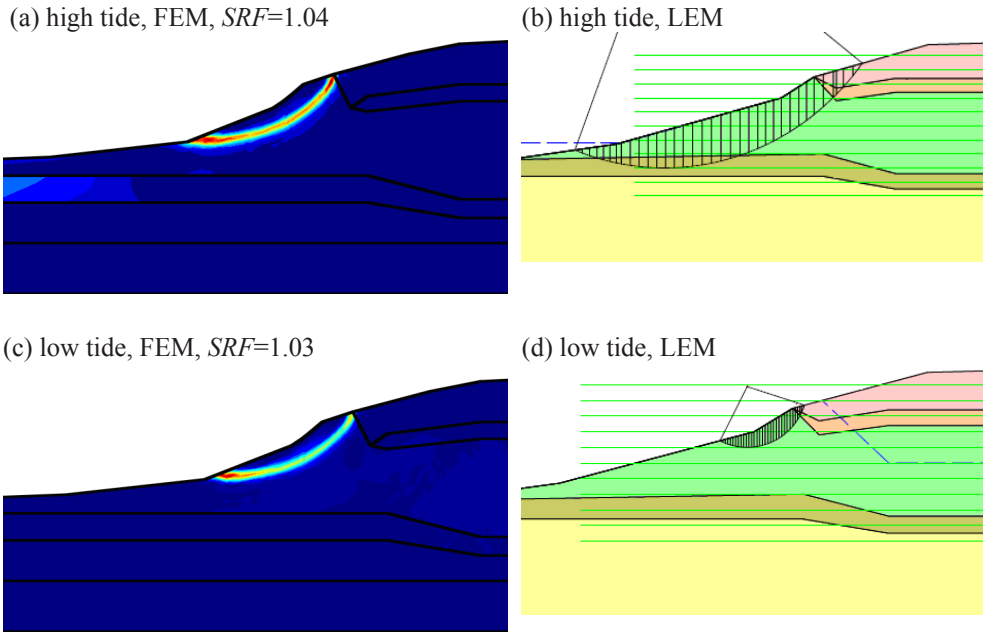

Figure 5-10. Slip surfaces; high tide: (a) FEM (strength parameters scaled by *SRF*=1.04), (b) LEM; low tide: (c) FEM (strength parameters scaled by *SRF*=1.03), (d) LEM

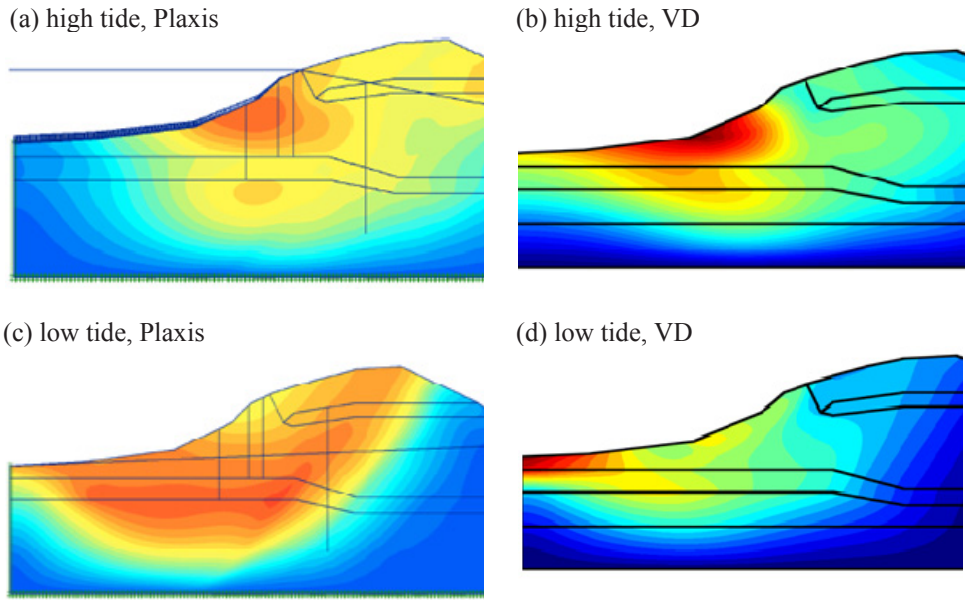

Figure 5-11. Comparison of total displacements; high tide: (a) Plaxis, (b) Virtual Dike; low tide: (c) Plaxis, (d) Virtual Dike

5.7 Conclusions

The first scientific question raised in this research was check of a principal ability of an earthen dike computational model to adequately simulate complex physical processes occurring at failure and correctly predict failure under prescribed loads. The Boston levee validation test site has become the next step towards the positive answer to this question.

The Boston dike analysis included cross-validation of the Virtual Dike module against two other models: a FEM model built in Plaxis software and a LEM model analyzed Geo-Stability software package. Two FEM models (Plaxis and Virtual Dike) have produced very close results, particularly, close values of strength reduction factors well (the difference is 6% and 5% for high tide and low tide, respectively). LEM analysis was a bit less precise: a typical LEM assumption on the hydrostatic distribution of pore pressures in the dike has become critical for the clayey Boston levee – the capillary fringe is very high in the dike and water storing effects must be taken into consideration (like it was done in *Virtual Dike* and Plaxis models).

Piezometers readings show that the massive soft brown clay layer stays fully saturated during tidal cycles and its condition is undrained. According to the stability analysis carried by finite element method and by Bishop's limit equilibrium method, slope failure occurs with the development of an approximately circular slip surface located in the soft brown clay layer. Both methods, LEM and FEM, confirm that the least stable hydraulic condition is the combination of the minimum river levels at low tide with the maximum saturation of soil layers. The factors of safety calculated by Bishop's limit equilibrium method are significantly higher than strength reduction factors calculated by FEM (by 22-100 %). In our case, the discrepancy between LEM and FEM results is predominantly due to the differences in calculation of hydraulic loads in the dike from tidal oscillations.

Virtual Dike results indicate that in real-life winter and spring conditions, the dike is almost at its limit state, at the margin of safety (strength reduction factor values are 1.03 and 1.04 for the low-tide and high-tide phases, respectively). These results agree well with the real-life observations, showing occasional slope failures at high tidal range.